β-decay rates of r-process nuclei in the relativistic quasiparticle random phase approximation

Nikšić, Tamara; Marketin, Tomislav; Vretenar, Dario; Paar, Nils; Ring, Peter

β-decay rates of r-process nuclei in the relativistic quasiparticle random phase approximation

T. Nikšić, T. Marketin, and D. Vretenar
Physics Department, Faculty of Science, University of Zagreb, Croatia

N. Paar
Institut für Kernphysik, Technische Universität Darmstadt, Schlossgartenstrasse 9, D-64289 Darmstadt, Germany

P. Ring
Physik-Department der Technischen Universität München, D-85748 Garching, Germany
(Received 30 August 2004; published 19 January 2005)

The fully consistent relativistic proton-neutron quasiparticle random phase approximation (PN-RQRPA) is employed in the calculation of β-decay half-lives of neutron-rich nuclei in the $N \approx 50$ and $N \approx 82$ regions. A new density-dependent effective interaction, with an enhanced value of the nucleon effective mass, is used in relativistic Hartree-Bogoliubov calculation of nuclear ground states and in the particle-hole channel of the PN-RQRPA. The finite range Gogny D1S interaction is employed in the $T = 1$ pairing channel, and the model also includes a proton-neutron particle-particle interaction. The theoretical half-lives reproduce the experimental data for the Fe, Zn, Cd, and Te isotopic chains but overestimate the lifetimes of Ni isotopes and predict a stable ^{132}Sn.

DOI: 10.1103/PhysRevC.71.014308 PACS number(s): 21.30.Fe, 21.60.Jz, 23.40.Hc, 26.30.+k

I. INTRODUCTION

The latest theoretical and computational advances in nuclear structure modeling have also had a strong impact on nuclear astrophysics. More and more often calculations of stellar nucleosynthesis, nuclear aspects of supernova collapse and explosion, and neutrino-induced reactions are based on microscopic global predictions for the nuclear ingredients rather than on oversimplified phenomenological approaches. The nuclear input for astrophysics calculations necessitates the properties of thousands of nuclei far from stability, including the characteristics of strong electromagnetic and weak interaction processes. Most of these nuclei, especially on the neutron-rich side, are not accessible in experiments and, therefore, many nuclear astrophysics calculations crucially depend on accurate theoretical predictions for the nuclear masses, bulk properties, nuclear excitations, (n, γ) and (γ, n) rates, α- and β-decay half-lives, fission probabilities, electron and neutrino capture rates, and so on.

The path of the r-process nucleosynthesis runs through regions of very neutron-rich nuclei. β decays are particularly important because they generate elements with higher Z values, and set the time scale of the r process. Except for a few key nuclei, however, β decays of r-process nuclei have to be determined from nuclear models. One of the crucial questions for structure models is, therefore, a consistent microscopic calculation of β decay far from stability. Two microscopic approaches have been successfully applied in large-scale modeling of weak interaction rates of neutron-rich nuclei: the shell model and the proton-neutron quasiparticle random phase approximation (PN-QRPA). Shell model applications in nuclear astrophysics have recently been reviewed in Ref. [1]. In the calculation of β half-lives, in particular, the principal advantage of the shell model is the ability to take into account the detailed structure of the β-strength functions. In addition to large-scale shell model predictions for the half-lives of waiting-point nuclei at $N = 50, 80, 126$ [1], the no-core shell model [2] and the shell model embedded in the continuum [3] have recently been applied to β decay of light nuclei. Large configuration spaces, however, prevent systematic applications of the shell model to heavy nuclei along the r-process path.

When compared to the shell model, important advantages of an QRPA approach based on the microscopic self-consistent mean-field framework, include the use of global effective nuclear interactions and the treatment of arbitrarily heavy systems. Fully self-consistent QRPA calculations of weak interaction rates of neutron-rich nuclei, however, have only recently been reported. In Ref. [4], in particular, a fully self-consistent QRPA has been formulated in Hartree-Fock-Bogoliubov (HFB) canonical single-particle basis. The canonical basis diagonalizes the density matrix and describes both the bound states and the positive-energy single-particle continuum. The formulation of the RQRPA in the canonical basis is particularly convenient because to describe transitions to low-lying states in weakly bound nuclei, the two-quasiparticle configuration space must include states with both nucleons in the discrete bound levels, states with one nucleon in a bound level and one nucleon in the continuum, and also states with both nucleons in the continuum. The HFB+QRPA model based on Skyrme interactions, and with the inclusion of a finite-range residual proton-neutron particle-particle interaction, has been applied in the calculation of β-decay rates for spherical neutron-rich r-process waiting-point nuclei [4]. Based on a different energy-density functional, the self-consistent HFB plus continuum QRPA framework has been employed in a systematic calculation of the allowed and first-forbidden β-decay rates for the r-process nuclei near $N = 50, 80, 126$ [5]. It has been shown that the effect of the high-energy

first-forbidden transitions is crucial for $Z \geqslant 50$, $N \approx 82$, and especially in the $N = 126$ region.

In this work we report the first application of the relativistic PN-QRPA in the calculation of β^--decay rates for neutron-rich nuclei. Self-consistent relativistic mean-field models have been very successfully applied to nuclear structure, not only in nuclei along the valley of β stability, but also in exotic nuclei with extreme isospin values and close to the particle drip lines. The relativistic mean-field framework has recently been extended to include medium dependent meson-nucleon vertices. One way to determine the functional form of the meson-nucleon vertices is from in-medium Dirac-Brueckner interactions, obtained from realistic free-space *NN* interactions. This microscopic method represents an *ab initio* description of nuclear matter and finite nuclei. Another approach is purely phenomenological, with the density dependence for the σ-, ω-, and ρ-meson-nucleon couplings adjusted to properties of nuclear matter and a set of spherical nuclei. The resulting density-dependent meson-nucleon couplings are in qualitative agreement with those obtained in the microscopic approach. In Ref. [6] we have extended the relativistic Hartree-Bogoliubov (RHB) model to include medium-dependent vertex functions. A phenomenological effective interaction, denoted DD-ME1, was adjusted to properties of nuclear matter and finite nuclei and tested in the analysis of the equations of state for symmetric and asymmetric nuclear matter, of ground-state properties of the Sn and Pb isotopic chains [6], and deformed nuclei [7]. It has been shown that, in comparison with standard nonlinear meson self-interactions, relativistic Lagrangians with an explicit density dependence of the meson-nucleon couplings provide an improved description of asymmetric nuclear matter, neutron matter, and nuclei far from stability. The relativistic random-phase approximation (RRPA), based on effective Lagrangians characterized by density-dependent meson-nucleon vertex functions, has been derived in Ref. [8]. In Ref. [9] the relativistic QRPA has been formulated in the canonical single-nucleon basis of the RHB model, and the corresponding proton-neutron relativistic QRPA (PN-RQRPA) has recently been employed in studies of isobaric analog resonances and Gamow-Teller resonances in spherical nuclei [10,11].

Our initial attempt to calculate β^--decay rates of r-process nuclei by simply employing the DD-ME1 interaction in the RHB plus PN-RQRPA framework was not successful. In general, the resulting half-lives were more than an order of magnitude longer than the empirical values. The reason is that DD-ME1, as well as most other successful relativistic mean-field interactions, has a relatively low effective nucleon mass, especially when compared to effective masses of Skyrme forces. This means that, because the density of states around the Fermi surface is low, in a self-consistent relativistic QRPA calculation of β decay the transition energies are low, and this result in long lifetimes. In some cases one could improve the results by adjusting the strength of the $T = 0$ pairing interaction, which is not really known, but this is not the solution of the problem, and in any case it cannot be applied to doubly closed-shell nuclei. The problem of adjusting the effective nucleon mass in relativistic mean-field models is somewhat complicated, because this quantity is also related to the energy spacings between spin-orbit partner states. Because the latter are empirically well determined, the effective nucleon mass cannot be increased without extending the standard relativistic mean-field framework. To be able to calculate β-decay half-lives, in this work we adjust a new relativistic mean-field density-dependent interaction with a higher value of the effective nucleon mass, by including an isoscalar tensor-coupling term in the model Lagrangian. In Sec. II we outline the theoretical framework and derive the new effective interaction DD-ME1*. In Sec. III the relativistic PN-QRPA is employed in the calculation of β-decay half-lives in the regions $N \approx 50$ and $N \approx 82$. Section IV contains the summary, concluding remarks, and an outlook of future applications.

II. OUTLINE OF THE THEORETICAL FRAMEWORK

A. Proton-neutron relativistic quasiparticle random-phase approximation

The relativistic QRPA has been derived in Ref. [9], in the canonical single-nucleon basis of the relativistic Hartree-Bogoliubov (RHB) model. The RHB model presents the relativistic extension of the Hartree-Fock-Bogoliubov framework, and it provides a unified description of *ph* and *pp* correlations. In the RHB framework the ground state of a nucleus can be written either in the quasiparticle basis as a product of independent quasiparticle states or in the canonical basis as a highly correlated BCS-state. By definition, the canonical basis diagonalizes the density matrix and it is always localized. It describes both the bound states and the positive-energy single-particle continuum. The matrix equations of the QRPA take a particularly simple form in the canonical basis, including only the matrix elements $V^{ph}_{\kappa\lambda'\kappa'\lambda}$ of the residual *ph* interaction and the matrix elements $V^{pp}_{\kappa\kappa'\lambda\lambda'}$ of the pairing *pp* interaction, as well as certain combinations of the occupation factors u_κ, v_κ of the canonical single-nucleon states. The RQRPA configuration space includes the Dirac sea of negative energy states. In addition to the configurations built from two-quasiparticle states of positive energy, the RQRPA configuration space must also contain pair-configurations formed from the fully or partially occupied states of positive energy and the empty negative-energy states from the Dirac sea. The inclusion of configurations built from occupied positive-energy states and empty negative-energy states is essential for current conservation and the decoupling of spurious states. In recent applications of the relativistic (Q)RPA it has been shown that the fully consistent inclusion of the Dirac sea of negative energy states in the R(Q)RPA configuration space is essential for a quantitative comparison with the experimental excitation energies of giant resonances [9,12,13].

The RHB+RQRPA model is fully self-consistent. For the interaction in the particle-hole channel effective Lagrangians with nonlinear meson self-interactions or density-dependent meson-nucleon couplings are used, and pairing correlations are described by the pairing part of the finite range Gogny interaction. In both the *ph* and *pp* channels, the same interactions are used in the RHB equations that determine

the canonical quasiparticle basis and in the matrix equations of the RQRPA. This is very important, because the energy weighted sum rules are satisfied only if the pairing interaction is consistently included both in the static RHB and in the dynamical RQRPA calculations. In both channels the same strength parameters of the interactions are used in the RHB and RQRPA calculations.

In Ref. [11] we have derived the matrix equations of the corresponding proton-neutron relativistic QRPA (PN-RQRPA) for an effective Lagrangian characterized by density-dependent meson-nucleon couplings. The PN-RQRPA has been applied in a study of charge-exchange modes: isobaric analog resonances and Gamow-Teller resonances. The model includes both the $T = 1$ and $T = 0$ pairing channels and presents a relativistic extension of the fully consistent proton-neutron QRPA that has been formulated in Ref. [4] and employed in an analysis of β-decay rates of r-process nuclei. To build a complete basis, the model space also includes configurations built from occupied positive-energy states and empty negative-energy states. It has been shown recently [11,14] that the total GT strength in the nucleon sector is reduced by $\approx$12% in nuclear matter and $\approx$6% in finite nuclei when compared to the Ikeda sum rule [15] as follows:

$$\left(S^{\rm GT}_{\beta^-} - S^{\rm GT}_{\beta^+}\right) = 3(N - Z), \tag{1}$$

where $S^{\rm GT}_{\beta^\pm}$ denotes the total sum of Gamow-Teller strength for the $\beta^\pm$-transition. The reduction has been attributed to the effect of Dirac sea negative-energy states, that is, the missing part of the sum rule is taken by configurations formed from occupied states in the Fermi sea and empty negative-energy states in the Dirac sea.

We consider transitions between the 0^+ ground state of a spherical even-even parent nucleus and the 1^+ excited state of the corresponding odd-odd daughter nucleus, which are induced by the Gamow-Teller operator $\boldsymbol{\sigma}\tau_-$. The matrix equations of the PN-RQRPA read as follows:

$$\begin{pmatrix} A & B \\ B^* & A^* \end{pmatrix} \begin{pmatrix} X^\lambda \\ Y^\lambda \end{pmatrix} = E_\lambda \begin{pmatrix} 1 & 0 \\ 0 & -1 \end{pmatrix} \begin{pmatrix} X^\lambda \\ Y^\lambda \end{pmatrix}. \tag{2}$$

The matrices A and B are defined in the canonical basis [16] as follows:

$$\begin{aligned} A_{pn,p'n'} &= H^{11}_{pp'}\delta_{nn'} + H^{11}_{nn'}\delta_{pp'} \\ &\quad + (u_p v_n u_{p'} v_{n'} + v_p u_n v_{p'} u_{n'}) V^{ph}_{pn'np'} \\ &\quad + (u_p u_n u_{p'} u_{n'} + v_p v_n v_{p'} v_{n'}) V^{pp}_{pnp'n'} \\ B_{pn,p'n'} &= (u_p v_n v_{p'} u_{n'} + v_p u_n u_{p'} v_{n'}) V^{ph}_{pp'nn'} \\ &\quad - (u_p u_n v_{p'} v_{n'} + v_p v_n u_{p'} u_{n'}) V^{pp}_{pnp'n'}. \end{aligned} \tag{3}$$

Here p, p', and n, n' denote proton and neutron quasiparticle canonical states, respectively, V^{ph} is the proton-neutron particle-hole residual interaction in the 1^+ channel, and V^{pp} is the corresponding particle-particle interaction. The canonical basis diagonalizes the density matrix, and the occupation amplitudes $v_{p,n}$ are the corresponding eigenvalues. However, the canonical basis does not diagonalize the Dirac single-nucleon mean-field Hamiltonian $\hat{h}_D$ or the pairing field $\hat{\Delta}$, and therefore the off-diagonal matrix elements $H^{11}_{nn'}$ and $H^{11}_{pp'}$ appear in Eq. (3):

$$H^{11}_{\kappa\kappa'} = (u_\kappa u_{\kappa'} - v_\kappa v_{\kappa'}) h_{\kappa\kappa'} - (u_\kappa v_{\kappa'} + v_\kappa u_{\kappa'}) \Delta_{\kappa\kappa'}. \tag{4}$$

For each energy E_λ, X^λ, and Y^λ in Eq. (3) denote the corresponding forward- and backward-going QRPA amplitudes, respectively. The total strength for the transition between the ground state of the even-even (N, Z) nucleus and a 1^+ state of the odd-odd $(N - 1, Z + 1)$ nucleus, induced by the Gamow-Teller operator, reads as follows:

$$B_\lambda = \left| \sum_{pn} < p||\boldsymbol{\sigma}\tau_-||n > \left(X^\lambda_{pn} u_p v_n - Y^\lambda_{pn} v_p u_n\right) \right|^2. \tag{5}$$

The spin-isospin-dependent interaction terms are generated by the π- and ρ-meson exchange. Although the direct one-pion contribution to the nuclear ground state vanishes at the mean-field level because of parity conservation, it has to be included in the calculation of spin-isospin excitations. The particle-hole residual interaction of the PN-RQRPA is derived from the Lagrangian density as follows:

$$\mathcal{L}^{\rm int}_{\pi+\rho} = -g_\rho \bar{\psi}\gamma^\mu \vec{\rho}_\mu \vec{\tau}\psi - \frac{f_\pi}{m_\pi} \bar{\psi}\gamma_5\gamma^\mu \partial_\mu \vec{\pi}\vec{\tau}\psi. \tag{6}$$

Vectors in isospin space are denoted by arrows, and boldface symbols will indicate vectors in ordinary three-dimensional space.

The coupling between the ρ-meson and the nucleon is assumed to be a vertex function of the baryon density. In Ref. [8] it has been shown that the explicit density dependence of the meson-nucleon couplings introduces additional rearrangement terms in the residual two-body interaction of the RRPA and that their contribution is essential for a quantitative description of excited states. However, because the rearrangement terms include the corresponding isoscalar ground-state densities, it is easy to see that they are absent in the charge exchange channel, and the residual two-body interaction reads as follows:

$$\begin{aligned} V(\boldsymbol{r}_1, \boldsymbol{r}_2) &= \vec{\tau}_1\vec{\tau}_2 (\beta\gamma^\mu)_1 (\beta\gamma_\mu)_2 g_\rho[\rho_v(\boldsymbol{r}_1)] g_\rho[\rho_v(\boldsymbol{r}_2)] \\ &\quad \times D_\rho(\boldsymbol{r}_1, \boldsymbol{r}_2) - \left(\frac{f_\pi}{m_\pi}\right)^2 \vec{\tau}_1\vec{\tau}_2 (\boldsymbol{\Sigma}_1\nabla_1)(\boldsymbol{\Sigma}_2\nabla_2) D_\pi(\boldsymbol{r}_1, \boldsymbol{r}_2). \end{aligned} \tag{7}$$

$D_{\rho(\pi)}$ denotes the meson propagator

$$D_{\rho(\pi)} = \frac{1}{4\pi} \frac{e^{-m_{\rho(\pi)}|\boldsymbol{r}_1 - \boldsymbol{r}_2|}}{|\boldsymbol{r}_1 - \boldsymbol{r}_2|}, \tag{8}$$

and

$$\boldsymbol{\Sigma} = \begin{pmatrix} \boldsymbol{\sigma} & 0 \\ 0 & \boldsymbol{\sigma} \end{pmatrix}. \tag{9}$$

For the ρ-meson coupling we adopt the functional form used in the DD-ME1 density-dependent effective interaction [6]

$$g_\rho(\rho_v) = g_\rho(\rho_{\rm sat}) \exp[-a_\rho(x - 1)], \tag{10}$$

where $x = \rho_v/\rho_{\rm sat}$ and $\rho_{\rm sat}$ denotes the saturation vector nucleon density in symmetric nuclear matter. For the pseudovector pion-nucleon coupling we use the following standard values:

$$m_\pi = 138.0\ {\rm MeV} \qquad \frac{f_\pi^2}{4\pi} = 0.08. \tag{11}$$

The derivative type of the pion-nucleon coupling necessitates the inclusion of the zero-range Landau-Migdal term, which accounts for the contact part of the nucleon-nucleon interaction

$$V_{\delta\pi} = g' \left(\frac{f_\pi}{m_\pi}\right)^2 \vec{\tau}_1\vec{\tau}_2 \mathbf{\Sigma}_1 \cdot \mathbf{\Sigma}_2 \delta(\boldsymbol{r}_1 - \boldsymbol{r}_2), \quad (12)$$

with the parameter g' adjusted to reproduce experimental data on the GTR excitation energies.

In the *pp* channel of the RHB model we have used a phenomenological pairing interaction, the pairing part of the Gogny force,

$$V^{pp}(1,2) = \sum_{i=1,2} e^{-[(\mathbf{r}_1-\mathbf{r}_2)/\mu_i]^2} \times (W_i + B_i P^\sigma - H_i P^\tau - M_i P^\sigma P^\tau), \quad (13)$$

with the set D1S [17] for the parameters μ_i, W_i, B_i, H_i, and M_i ($i = 1, 2$). This force has been very carefully adjusted to the pairing properties of finite nuclei all over the periodic table. In particular, the basic advantage of the Gogny force is the finite range, which automatically guarantees a proper cut-off in momentum space. For the $T = 0$ proton-neutron pairing interaction in open shell nuclei we employ a similar interaction that was used in the nonrelativistic QRPA calculation [4] of β-decay rates for spherical neutron-rich r-process waiting-point nuclei. It consists of a short-range repulsive Gaussian combined with a weaker longer-range attractive Gaussian as follows:

$$V_{12} = -V_0 \sum_{j=1}^{2} g_j \, e^{-r_{12}^2/\mu_j^2} \hat{\Pi}_{S=1,T=0}, \quad (14)$$

where $\hat{\Pi}_{S=1,T=0}$ projects onto states with $S = 1$ and $T = 0$. We follow the prescription from Ref. [4] and take the ranges $\mu_1 = 1.2$ fm and $\mu_2 = 0.7$ fm of the two Gaussians from the Gogny interaction (13). The relative strengths $g_1 = 1$ and $g_2 = -2$ are chosen so that the force is repulsive at small distances. The overall strength of the force represents the only remaining free parameter. We have already successfully applied this force in an analysis of the Gamow-Teller resonances in tin isotopes [11].

B. Calculation of β-decay half-lives

The rate for the decay of an even-even nucleus in the allowed Gamow-Teller approximation reads as follows:

$$\frac{1}{T_{1/2}} = \sum_m \lambda_{if}^m = D^{-1} g_A^2 \sum_m \int dE_e \left| \sum_{pn} \langle 1_\lambda^+ || \sigma\tau_- || 0^+ \rangle \right|^2 \frac{dn_m}{dE_e}, \quad (15)$$

where $D = 6163.4 \pm 3.8$ s [18]. $|0^+\rangle$ denotes the ground state of the parent nucleus, and $|1_\lambda^+\rangle$ is a state of the daughter nucleus. The sum runs over all final states with an excitation energy smaller than the Q_{β^-} value. To account for the universal quenching of the Gamow-Teller strength function, we use the effective weak axial nucleon coupling constant $g_A = 1$, instead of $g_A = 1.26$ [19]. The kinematic factor in Eq. (15) can be written as follows:

$$\frac{dn_m}{dE_e} = E_e \sqrt{E_e^2 - m_e^2} (\omega - E_e)^2 F(Z, A, E_e), \quad (16)$$

where ω denotes the energy difference between the initial and the final state. The Fermi function $F(Z, A, E_e)$ corrects the phase-space factor for the nuclear charge and finite nuclear size effects [20].

C. The nucleon effective mass in the RMF models

In nonrelativistic mean-field models the effective nucleon mass m^* characterizes the energy dependence of an effective local potential that is equivalent to the nonlocal and frequency-dependent microscopic nuclear potential [21]. m^* represents a measure of the density of single-nucleon states around the Fermi surface and, therefore, it has a pronounced effect on the calculated properties of ground and excited states. In the case of Skyrme-type interactions, for instance, calculation of ground-state properties and excitation energies of quadrupole giant resonances have shown that a realistic choice for the nucleon effective mass is in the interval $m^*/m = 0.8 \pm 0.1$ [22].

In the relativistic mean-field framework the expression "effective mass" has been used to denote different quantities. The quantity which is usually used to characterize an effective interaction, and which in the literature is most often called "the relativistic effective mass," is also known as the "Dirac mass" [23]

$$m_D = m + S(\boldsymbol{r}), \quad (17)$$

where m is the bare nucleon mass and $S(\boldsymbol{r})$ denotes the scalar nucleon self-energy. The concept of the effective nucleon mass in the relativistic framework has been extensively analyzed in Refs. [23,24]. Specifically, it has been pointed out that the Dirac mass should not be identified with the effective mass of the nonrelativistic mean-field models. Instead, the quantity which should be compared with the empirical effective mass derived from the nonrelativistic analyses of scattering and bound state data is given by the following:

$$m^*/m = 1 - V/m, \quad (18)$$

where V denotes the timelike component of the vector self-energy. The Dirac mass, conversely, is determined by two factors: (i) the empirical spin-orbit splittings in finite nuclei and (ii) the binding energy at the saturation density in nuclear matter. In the first order approximation, and assuming spherical symmetry, the spin-orbit part of the effective single-nucleon potential reads as follows:

$$V_{\text{S.O.}}(r) = \frac{1}{4\bar{M}^2} \left(\frac{1}{r}\frac{d}{dr}(V - S)\right) \boldsymbol{l} \cdot \boldsymbol{\sigma}, \quad (19)$$

where $\bar{M}$ is specified as follows:

$$\bar{M} = M - \tfrac{1}{2}(V - S). \quad (20)$$

Although the difference between the vector and scalar potentials determines the spin-orbit potential, their sum defines

the effective single-nucleon potential and is determined by the nuclear matter binding energy at saturation density. The energy spacings between spin-orbit partner states in finite nuclei, and the nuclear matter binding and saturation, place the following constraints on the values of the Dirac mass and the nucleon effective mass: $0.55m \leqslant m_D \leqslant 0.6m$, $0.64m \leqslant m^* \leqslant 0.67m$, respectively. These values have been used in most standard relativistic mean-field effective interactions. First, we notice that in comparison to the nonrelativistic models, the relativistic nucleon effective mass has a rather low value, and this results in a smaller density of states around the Fermi surface. Second, the range of allowed values of the nucleon effective mass is very narrow in the standard relativistic mean-field phenomenology, and there is really no room for any significant enhancement of the single-nucleon level densities at the Fermi surface.

In Ref. [25] we have extended the standard relativistic mean-field model by including dynamical effects originating from the coupling of single-nucleon motion to collective surface vibrations. By using a simple linear ansatz for the energy dependence of the scalar and vector nucleon self-energies, we were able to describe simultaneously bulk nuclear properties and single-nucleon spectra in a self-consistent relativistic framework.

As we have emphasized in the introduction, to be able to reproduce the data on β-decay lifetimes, the description of single-particle energies around the Fermi surface has to be improved. In principle one could use the method of Ref. [25] with energy-dependent nucleon self-energies, but here we will try a simpler approach to increase the density of single-nucleon states without going beyond mean-field level. An increase of the effective mass necessitates a reduction of the vector self-energy [see Eq. (18)]. However, to retain the empirical value of the nuclear matter binding energy, the scalar self-energy should be reduced correspondingly. A serious problem arises because such an effective interaction would systematically underestimate the spin-orbit splittings in finite nuclei. A solution to this problem has been known for a long time, namely the tensor coupling of the ω-meson to the nucleon. This interaction enhances the effective spin-orbit potential in finite nuclei but is not included in the most commonly used relativistic mean-field models. In Ref. [26] it was shown that the following tensor coupling:

$$\mathcal{L}_{\text{tensor}} = -\frac{f_V}{2M}\bar{\psi}\sigma^{\mu\nu}\psi(\partial_\mu\omega_\nu - \partial_\nu\omega_\mu), \tag{21}$$

generates an additional term in the spin-orbit part of the effective nucleon potential, which now reads as follows:

$$V_{\text{S.O.}}(r) = \left[\frac{1}{4\bar{M}^2}\frac{1}{r}\frac{d}{dr}(V - S) + \frac{f_V}{2M\bar{M}}\frac{1}{r}\frac{d\omega}{dr}\right]\boldsymbol{l}\cdot\boldsymbol{\sigma}. \tag{22}$$

With the inclusion of the tensor ω-nucleon coupling it becomes possible to reproduce the empirical spin-orbit splittings, even when using effective interactions with the Dirac mass as large as $m_D \approx 0.7m$.

Our strategy is now to use the additional tensor-coupling term to generate a density-dependent relativistic effective interaction, with a value for the effective mass close to those used in nonrelativistic mean-field models. Starting from the DD-ME1 interaction that we have used in the PN-RQRPA analysis of charge-exchange modes [11], and with the inclusion of the additional tensor ω-nucleon interaction (21), the parameters of the new interaction have been adjusted simultaneously to properties of nuclear matter and finite nuclei [6]. An additional constraint has been placed on the value of the nucleon effective mass. The modified effective interaction, denoted as DD-ME1*, exhibits the following values for the Dirac mass and the nucleon effective mass: $m_D = 0.67m$, $m^* = 0.76m$, respectively. These are the highest values for which a realistic description of nuclear matter and finite nuclei is still possible, that is, the quality of the calculated nuclear matter equation of state and of ground-state properties of spherical nuclei is comparable to that of the DD-ME1 interaction. The value of the Dirac mass is also in agreement with the results of Ref. [26], where a detailed analysis was performed on the correlation between the isoscalar tensor coupling and the Dirac mass in successful mean-field models. Although the value of m^* is still lower than those typically used in nonrelativistic mean-field models, this result presents a significant improvement over the standard DD-ME1 density-dependent interaction ($m_D = 0.58m$, $m^* = 0.66m$).

TABLE I. Energy separation (in MeV) between spin-orbit partner states in doubly closed-shell nuclei, calculated with the DD-ME1 and DD-ME1* interactions and compared with experimental data [32].

		DD-ME1	DD-ME1*	Exp.
^{16}O	$\nu 1p$	6.32	6.02	6.18
	$\pi 1p$	6.25	5.96	6.32
^{40}Ca	$\nu 1d$	6.57	6.59	6.00
	$\pi 1d$	6.51	6.51	6.00
^{48}Ca	$\nu 1f$	7.69	7.79	8.38
	$\nu 2d$	1.72	0.56	2.02
^{132}Sn	$\nu 2d$	1.88	2.03	1.65
	$\pi 1g$	6.24	6.57	6.08
	$\pi 2d$	1.82	1.98	1.75
^{208}Pb	$\nu 2f$	2.20	2.38	1.77
	$\nu 1i$	6.84	7.13	5.84
	$\nu 3p$	0.88	0.89	0.90
	$\pi 2d$	1.65	1.82	1.33
	$\pi 1h$	5.84	6.06	5.56

We have used the new interaction to calculate the energy spacings between spin-orbit partner states in the doubly closed-shell nuclei ^{16}O, ^{40}Ca, ^{48}Ca, ^{132}Sn, and ^{208}Pb. The results are shown in Table I, in comparison with those obtained using the DD-ME1 interaction, and with the experimental data. Both interactions provide an excellent description of the spin-orbit splittings in finite nuclei. To illustrate the effect of the tensor-coupling term, in Fig. 1 we display the radial dependence of the spin-orbit term of the single-nucleon potential in the self-consistent solutions for the ground state of ^{132}Sn, calculated with the DD-ME1 and DD-ME1* effective interactions. For DD-ME1*, in particular, the contributions of the first and second term in Eq. (22) are also plotted separately. We notice that even though the strength of the

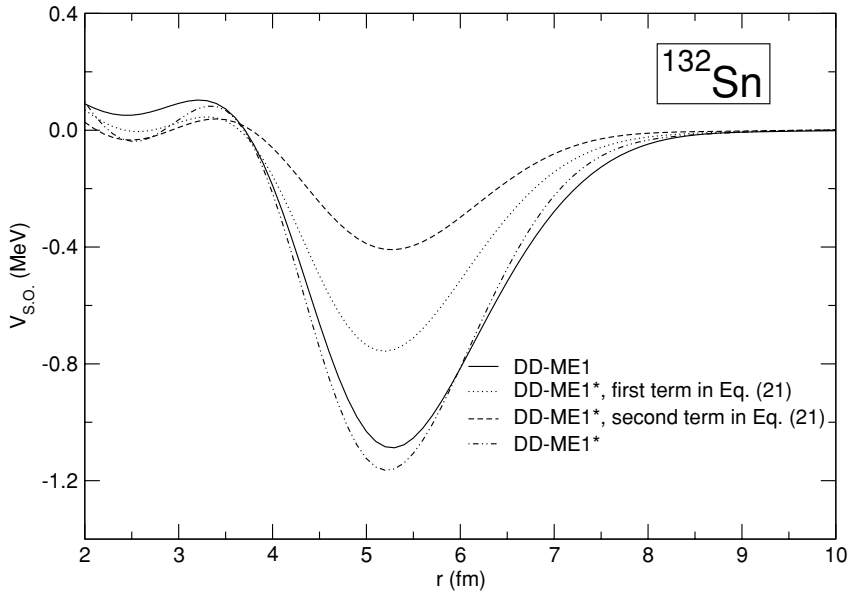

FIG. 1. Radial dependence of the spin-orbit term of the single-nucleon potential in self-consistent solutions for the ground state of ^{132}Sn. The curves correspond to RMF calculations with the DD-ME1 and DD-ME1* effective interactions. For the latter the contributions of the first and second term in Eq. (22) are plotted separately.

spin-orbit interaction that arises from the large scalar and vector self-energies [first term in Eq. (22)] is significantly reduced, the tensor ω-nucleon coupling effectively compensates this reduction, and the resulting spin-orbit potential is even slightly stronger than the one calculated with the DD-ME1 interaction. Therefore, although both interactions produce very similar results for the spin-orbit splittings in finite nuclei, the inclusion of the isoscalar tensor-coupling term in DD-ME1* allows for an increase of the Dirac mass and effective mass.

In Figs. 2 and 3 we display the neutron and proton single-particle levels in ^{78}Ni and ^{132}Sn, respectively, calculated with DD-ME1, DD-ME1*, and two nonrelativistic Skyrme interactions that have been used in the calculation of β-decay half-lives: SkO' [4] and SkSC17 [18]. Both nonrelativistic interactions are characterized by large values of the nucleon effective mass: $m^* = 0.89$ for SkO' and $m^* = 1.0$ for SkSC17. Compared to the original DD-ME1 interaction, the enhancement of the effective mass in DD-ME1* results in the increase of the density of states around the Fermi surface, similar to the spectra calculated with the nonrelativistic interactions. In Table II we compare the calculated neutron and proton single-particle levels in ^{132}Sn, with experimental data. The levels calculated with DD-ME1* are in much better agreement with data [27] than those obtained with the original DD-ME1 interaction.

In Fig. 4 we plot the evolution of the $\pi 2p_{3/2}$ and $\pi 1f_{5/2}$ single-particle levels in heavy copper isotopes. The level structure has been studied in a recent experiment [28], and it has been pointed out that a possible reordering of these proton levels could have a pronounced effect on the shell structure and decay properties for nuclei near and beyond the doubly magic ^{78}Ni. The results calculated with the DD-ME1* interaction

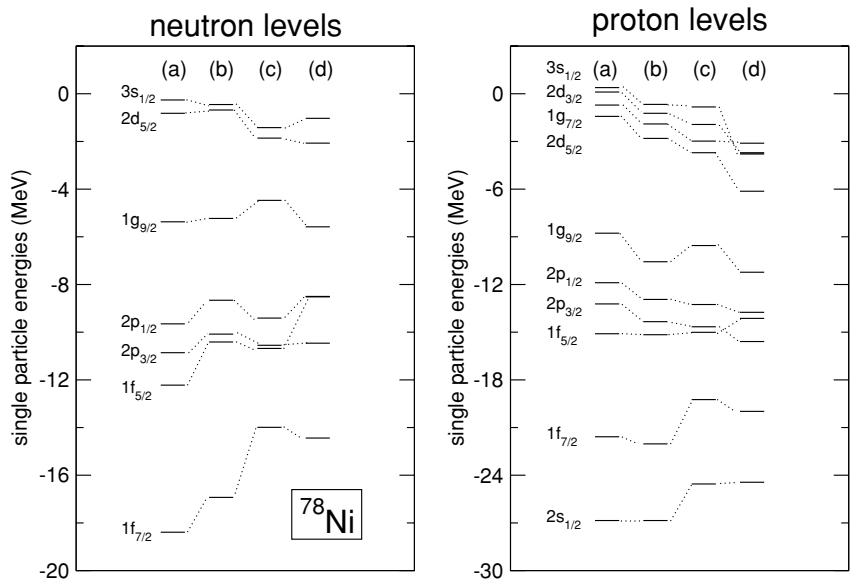

FIG. 2. Neutron and proton single-particle levels in ^{78}Ni calculated with DD-ME1 (a), DD-ME1* (b), and with two nonrelativistic Skyrme interactions: SkO' [4] (c) and SkSC17 [18] (d).

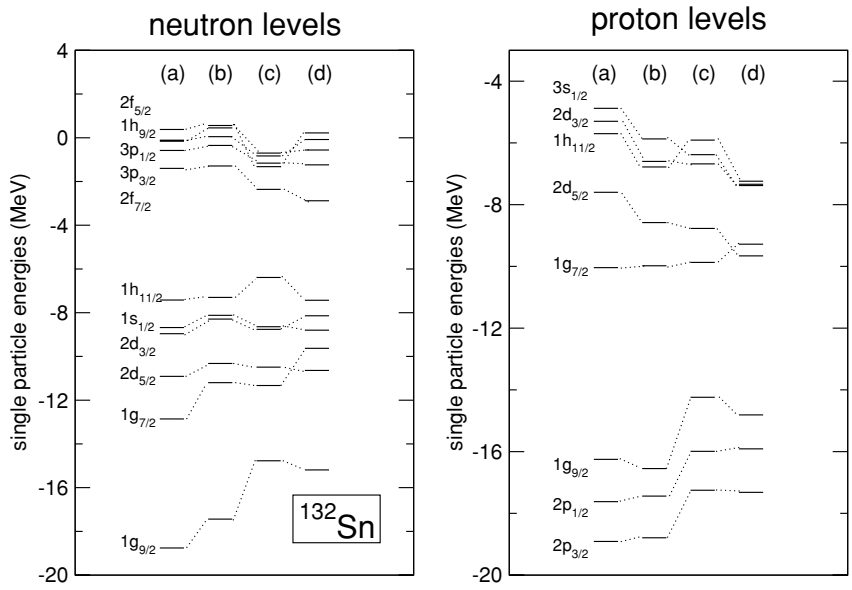

FIG. 3. Same as in Fig. 2 for ^{132}Sn.

are in excellent agreement with the experimental data. The model reproduces the observed lowering of the $\pi 1f_{5/2}$ state in ^{69}Cu, ^{71}Cu, and ^{73}Cu. For the heavier isotopes, experimental data are not yet avaliable. Nevertheless, our calculation predicts a further lowering of the $\pi 1f_{5/2}$ state, and already in the ^{75}Cu isotope the $\pi 1f_{5/2}$ state becomes the ground state.

III. β-DECAY HALF-LIVES

In Ref. [11] we have employed the proton-neutron RQRPA in a study of the high-energy part of the GT strength function, in particular the GT resonance that represents a coherent superposition of high-lying proton-particle/neutron-hole configurations associated with charge-exchange excitations from $j = l + \frac{1}{2}$ neutron orbitals into $j = l - \frac{1}{2}$ proton orbitals. In addition to the high-energy resonance, the GT strength function displays a concentration of strength in the region of low-energy excitations. These transitions correspond to core-polarization ($j = l \pm \frac{1}{2} \rightarrow j = l \pm \frac{1}{2}$), and back spin-flip ($j = l - \frac{1}{2} \rightarrow j = l + \frac{1}{2}$) neutron-hole/proton-particle excitations. It is precisely this low-energy tail that contributes to the β-decay process.

Only the isovector channel of the effective interaction contributes to the matrix elements of the residual interaction in the calculation of charge-exchange excitations. Nevertheless, the isoscalar channel plays an important role because it determines the single-particle levels that enter the PN-RQRPA calculations. In the analysis of charge-exchange modes we have used the DD-ME1 effective interaction, combined with the standard parameters for the pion-nucleon Lagrangian: $m_\pi = 138$ MeV and $f_\pi^2/4\pi = 0.08$. The parameter of the

TABLE II. Neutron (left panel) and proton (right panel) single-particle energies E_{nlj} in ^{132}Sn. For each panel, the left-hand column specifies the radial, orbital, and total angular momentum quantum numbers, the column labeled DD-ME1 contains results calculated with the standard density-dependent RMF interaction DD-ME1, and the spectrum calculated with the new effective interaction DD-ME1* is included in the third column. The theoretical spectra are compared to the experimental energies shown in the column labeled EXP.

Neutron states				Proton states			
nlj	DD-ME1	DD-ME1*	EXP	nlj	DD-ME1	DD-ME1*	EXP
$1g_{9/2}$	−18.76	−17.44		$2p_{3/2}$	−18.91	−18.79	
$2d_{5/2}$	−10.91	−10.32	−9.04	$2p_{1/2}$	−17.62	−17.44	−16.13
$1g_{7/2}$	−12.86	−11.20	−9.82	$1g_{9/2}$	−16.25	−16.55	−15.78
$3s_{1/2}$	−8.68	−8.12	−7.72	$1g_{7/2}$	−10.04	−9.98	−9.65
$1h_{11/2}$	−7.42	−7.30	−7.63	$2d_{5/2}$	−7.60	−8.58	−8.69
$2d_{3/2}$	−8.96	−8.29	−7.39	$2d_{3/2}$	−5.70	−6.60	−6.95
$2f_{7/2}$	−1.40	−1.29	−2.45	$1h_{11/2}$	−5.30	−6.78	−6.86
$3p_{3/2}$	−0.58	−0.35	−1.59	$3s_{1/2}$	−4.88	−5.87	
$1h_{9/2}$	−0.11	0.45	−0.88	$2f_{7/2}$	2.66	1.32	
$3p_{1/2}$	−0.16	0.05	−0.75				
$2f_{5/2}$	0.38	0.56	−0.44				

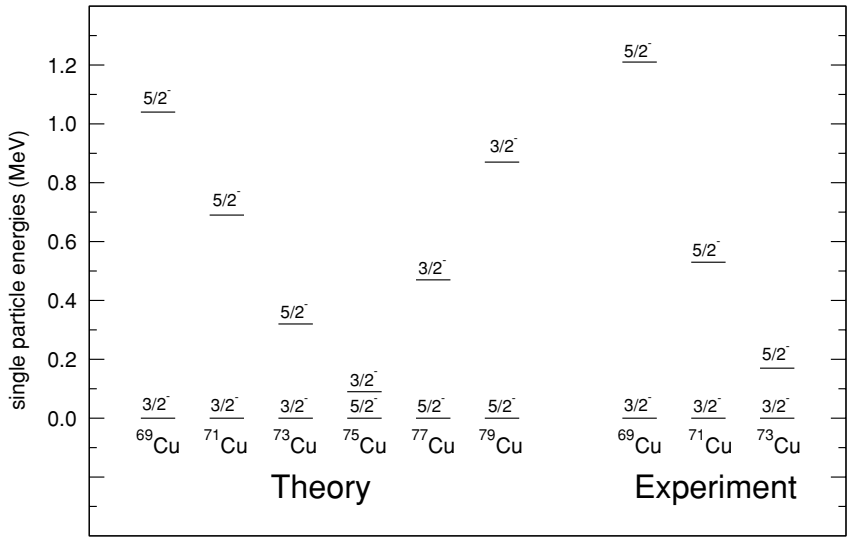

FIG. 4. $\pi 2p_{3/2}$ and $\pi 1f_{5/2}$ single-particle levels in heavy copper isotopes, calculated with the DD-ME1* interaction in comparison with experimental data [28].

zero-range Landau-Migdal force $g' = 0.55$ has been adjusted to reproduce the excitation energy of the GT resonance in ^{208}Pb. We have shown that, although the inclusion of $T = 0$ pairing in the residual interaction does affect both the low- and high-energy regions of the GT strength distribution, the position of the resonance is not sensitive to its strength [11]. Conversely, $T = 0$ pairing has a very strong influence on the low-lying tail of the GT strength distribution.

Our first attempt to apply the PN-RQRPA to β-decay processes, by employing the DD-ME1 interaction, was not successful. We tried to reproduce the empirical half-life of the ^{78}Ni. This spherical nucleus undergoes high-energy fast β decay and, because it has doubly closed spherical shells, there is no contribution from the $T = 0$ pairing. The PN-RQRPA with the DD-ME1 interaction predicts a half-life $T_{1/2} = 7$ s, which is an order of magnitude longer than the experimental value $T_{1/2} = 104 + 126 - 57$ ms [29]. The results of nonrelativistic QRPA calculations are much closer to the empirical half-life. For example, for the interaction DF3 the calculated half-life is $T_{1/2} \approx 0.3$ s [5], whereas the Skyrme interaction SkO' predicts $T_{1/2} \approx 0.6$ s [4]. Obviously, although the DD-ME1 interaction provides an accurate description of the high-energy region of the GT strength function, it does a rather poor job for the low-energy tail of the distribution. The problem, as we have already emphasized, lies in the low density of single-proton states around the Fermi level. This has motivated the adjustment of the new effective interaction DD-ME1*, which has a considerably higher value of the nucleon effective mass and consequently produces a higher density of single-nucleon states at the Fermi surface.

The change of the density of single-nucleon states will also affect the position of the GT resonance, and therefore the parameter of the zero-range Landau-Migdal force has to be readjusted. A higher density of states implies a lowering of the GT strength distribution, and this means that value of $g' = 0.55$ used with DD-ME1 has to be increased to reproduce the empirical excitation energy of GT resonances. For DD-ME1* we have adjusted the new value $g' = 0.62$ to the position of the GT resonance in ^{208}Pb. With this value of g' we also find an excellent agreement between the calculated and experimental excitation energies of the GTR for ^{48}Ca, ^{90}Zr, and $^{112-124}$Sn.

With the new set of parameters (DD-ME1* effective interaction, $m_\pi = 138$ MeV, $f_\pi^2/4\pi = 0.08$, $g' = 0.62$), we have recalculated the β-decay half-life of ^{78}Ni. The value $T_{1/2} = 0.9$ s presents a significant improvement over our first result obtained with DD-ME1, although it still overestimates the empirical half-life of ^{78}Ni and the values calculated with the nonrelativistic PN-QRPA. The most probable reason is that the value of the nucleon effective mass used in DD-ME1* is still below the values used in the nonrelativistic effective interactions [4,5]. A further increase of m^* in our relativistic model is, however, not possible without downgrading the agreement with experimental data on ground state properties of finite nuclei.

In recent years a number of experimental and theoretical studies have focused on the level structure and decay properties of neutron-rich nuclei in the vicinity of the doubly magic ^{78}Ni and ^{132}Sn. In particular, β-decay rates in these two regions of the periodic chart have been extensively investigated in the framework of the nonrelativistic PN-QRPA [4,5,18]. In the next two sections we apply the newly formulated relativistic PN-QRPA in the calculation of β-decay half-lives of nuclei in the regions $N \approx 50$ and $N \approx 82$.

A. $N \approx 50$ region

In this region we have investigated the iron, nickel, and zinc isotopic chains and the $N = 50$ isotones. The structure of the low-energy part of the GT strength distribution crucially depends on the occupancy of the $Z = 28$ proton shell. It should be noted that, because of possible deformation effects in the Fe and Zn chains, these nuclei might not be as good as the Ni isotopes for a comparison with results of spherical PN-QRPA calculations.

In Fig. 5 we display the calculated half-lives of the Fe isotopes (two holes in the $\pi 1f_{7/2}$ orbit) in comparison with the available experimental data [30]. The results are obtained with

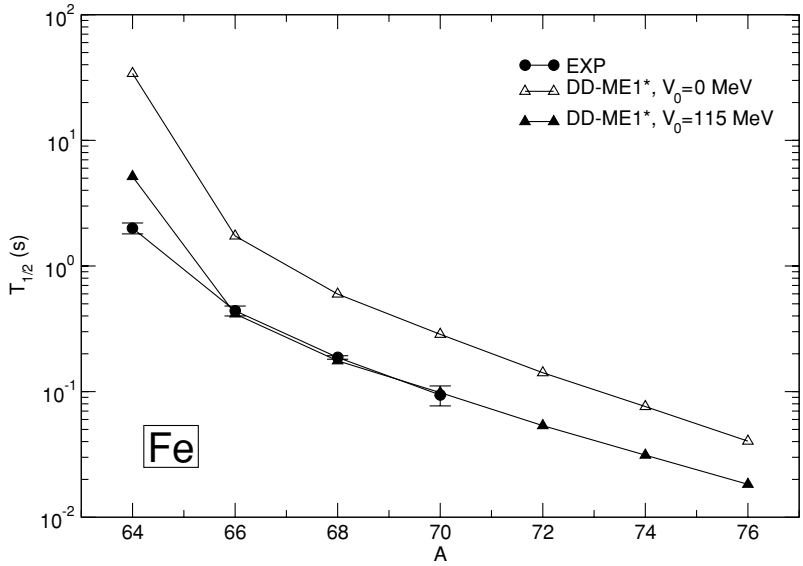

FIG. 5. Comparison of the calculated half-lives of Fe isotopes, for two values of the $T = 0$ pairing strength, with available experimental data [30].

the DD-ME1* interaction, $m_\pi = 138$ MeV, $f_\pi^2/4\pi = 0.08$, $g' = 0.62$, Gogny D1S $T = 1$ pairing. Two values for the strength parameter of the $T = 0$ pairing interaction (14) have been used. Obviously, the absolute values of the calculated half-lives are very sensitive to the $T = 0$ pairing strength. Without the inclusion of this pairing channel, in all considered cases the calculated half-lives are at least an order of magnitude longer than the experimental values. In the case of iron isotopes the pairing strength parameter $V_0 = 115$ MeV has been adjusted to reproduce the half-life of ^{68}Fe. With this value we are able to reproduce the half-lives of the ^{66}Fe and ^{70}Fe isotopes very accurately, whereas the lifetime of the ^{64}Fe isotope is somewhat overestimated.

It is, however, probable that the inclusion of a strong $T = 0$ pairing partially compensates the deficiencies of the single-particle spectra calculated with the DD-ME1* interaction. For the semimagic nucleus ^{76}Fe, in Fig. 6 we plot the probabilities λ_{fi} of β transitions from an initial nuclear state i to a final state f for different values of the $T = 0$ pairing strength. The ground-state occupation probabilities for the single-particle levels relevant for this β-decay process are listed in Table III. Because the $\pi 1f_{7/2}$ orbit is not fully occupied, the transition with the highest probability is dominated (95% of the neutron-to-proton QRPA amplitude) by the back spin-flip configuration $\nu 1f_{5/2} \to \pi 1f_{7/2}$. Other transitions, with much smaller probabilities, correspond to the back spin-flip configuration $\nu 2p_{1/2} \to \pi 2p_{3/2}$ and the core-polarization configurations $\nu 1f_{5/2} \to \pi 1f_{5/2}$, $\nu 1g_{9/2} \to \pi 1g_{9/2}$, $\nu 2p_{3/2} \to \pi 2p_{3/2}$, and $\nu 2p_{1/2} \to \pi 2p_{1/2}$. Because except $\pi 1f_{7/2}$, all proton single-particle levels listed in Table III have very small occupation probabilities, the only sizable contribution from the $T = 0$ pairing to the RQRPA matrices comes from the $\pi 1f_{7/2}(\nu 1f_{5/2})^{-1}$ pair. Because of the attractive nature of the pairing interaction, the large diagonal matrix element $v_p^2 V_{pnpn}^{pp}$ (p and n denote $\pi 1f_{7/2}$ and $\nu 1f_{5/2}$ states, respectively) effectively reduces the sum of the quasiparticle energies: $H_{pp}^{11} + H_{nn}^{11} = E_p + E_n$. This means that the $T = 0$ pairing compensates for the fact that even the DD-ME1* interaction still predicts a rather low density of states around the Fermi surface, that is, the $\pi 1f_{7/2}$ and $\nu 1f_{5/2}$ single-particle levels are still too close. The inclusion of the $T = 0$ pairing will affect only configurations with the proton level at least partially occupied. This is clearly seen

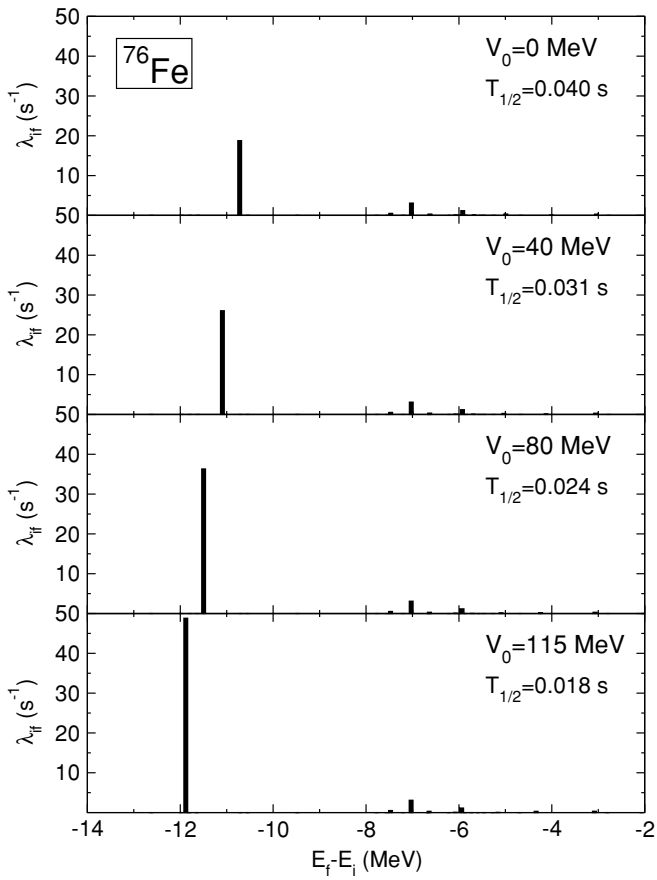

FIG. 6. Probabilities of β transitions for the semimagic ^{76}Fe for different values of the $T = 0$ pairing strength.

TABLE III. Occupation probabilities of neutron and proton single-particle states for the ground states of ^{76}Fe and ^{80}Zn.

	^{76}Fe		^{80}Zn		
nlj	Neutrons	Protons	nlj	Neutrons	Protons
$1f_{7/2}$	1.000	0.743	$1f_{7/2}$	1.000	0.980
$1f_{5/2}$	1.000	0.019	$1f_{5/2}$	1.000	0.260
$2p_{3/2}$	1.000	0.005	$2p_{3/2}$	1.000	0.098
$2p_{1/2}$	1.000	0.004	$2p_{1/2}$	1.000	0.040
$1g_{9/2}$	1.000	0.004	$1g_{9/2}$	1.000	0.014

in Fig. 6, where we notice that only the transition built from the configuration $\nu 1f_{5/2} \rightarrow \pi 1f_{7/2}$ is lowered in energy and enhanced with the increase of the strength of $T = 0$ pairing, whereas the remaining transitions are unaltered.

For the Ni isotopes the $\pi 1f_{7/2}$ orbit is completely occupied, that is, in this case the transition $\nu 1f_{5/2} \rightarrow \pi 1f_{7/2}$ is blocked. The $T = 0$ pairing could have an effect only on the $\pi 1g_{9/2}(\nu 1g_{9/2})^{-1}$ configuration, because the $\nu 1g_{9/2}$ orbit is not fully occupied for isotopes below ^{78}Ni. However, it is true that when this orbit is almost empty (^{70}Ni, ^{72}Ni) there is a large contribution from the pairing interaction, but at the same time there is only a small number of neutrons that can participate in the β-decay process. Conversely, when this orbit is almost full (^{74}Ni, ^{76}Ni), the contribution from the $T = 0$ pairing becomes negligible. In contrast to the iron isotopic chain, we were not able to obtain a single value of the $T = 0$ pairing strength parameter that would provide a consistent description of the entire chain of nickel isotopes. To reproduce the experimental half-lives, an extremely strong $T = 0$ pairing would have to be used and this would cause the collapse of the PN-RQRPA calculation. Because of the closed $Z = 28$ proton shell, the $T = 0$ pairing is not effective in Ni isotopes and, therefore, the calculated β-decay half-lives, shown in Fig. 7, overestimate the experimental data.

In this mass region we have also analyzed the half-lives of zinc isotopes. In Ref. [4] the measured half-lives of three zinc isotopes ^{76}Zn, ^{78}Zn, and ^{80}Zn, and of ^{82}Ge, were used to adjust the $T = 0$ pairing strength. It was shown that the experimental lifetimes can all be reproduced with a single value of the $T = 0$ pairing strength, $V_0 = 230$ MeV. In the present calculation the measured half-lives are only reproduced by using a much stronger $T = 0$ pairing interaction. The effect that $T = 0$ pairing has on the β-decay probability is illustrated in the example of the semimagic nucleus ^{80}Zn. In Table III the ground-state occupation probabilities for the relevant single-particle levels are included. It is important to note that, because of the $T = 1$ pairing, the occupation probability of the $\pi 1f_{7/2}$ state is not equal to 1. In addition to $\pi 1f_{7/2}$, only $\pi 1f_{5/2}$ has a sizable occupation probability among the proton states. The $T = 0$ pairing interaction produces a large contribution to the RQRPA matrices for the following configurations: $\pi 1f_{5/2}(\nu 1f_{5/2})^{-1}$ and $\pi 1f_{7/2}(\nu 1f_{5/2})^{-1}$. Because the transition $\nu 1f_{5/2} \rightarrow \pi 1f_{7/2}$ is essentially blocked, the effect of $T = 0$ pairing is much weaker than in the case of Fe isotopes. If the parameter V_0 is kept below $\approx$250 MeV, the $T = 0$ pairing has virtually no effect on the calculated half-lives. In the interval between $V_0 = 0$ MeV and $V_0 =$ 220 MeV the half-life decreases by just 10%. With a further increase of V_0, however, the calculated half-life displays a steep decrease. The measured half-life is reproduced for $V_0 \approx$ 330 MeV. The corresponding distributions of neutron-to-proton QRPA amplitudes for three values of the $T = 0$ pairing strength ($V_0 = 0$ MeV, $V_0 = 255$ MeV, and $V_0 = 330$ MeV) are shown in Table IV. As one would expect, in the absence of $T = 0$ pairing, the β-decay process is characterized by two transitions. The lower one is dominated by the back spin-flip transition $\nu 2p_{1/2} \rightarrow \pi 2p_{3/2}$, whereas the higher component represents a mixture of core-polarization transitions. Increasing the $T = 0$ pairing strength to $V_0 = 255$ MeV, we note that (i) transitions built from the back spin-flip configuration $\nu 2p_{1/2} \rightarrow \pi 2p_{3/2}$ and the core-polarization configurations are

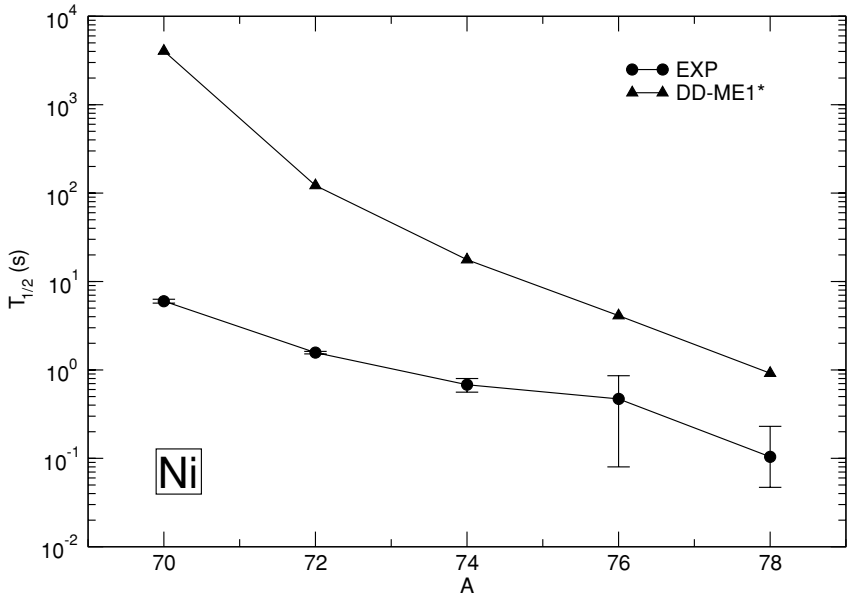

FIG. 7. Calculated half-lives of Ni isotopes, in comparison with experimental values. The data are from Ref. [30], except for ^{78}Ni where the value $T_{1/2} = 104 + 126 - 57$ ms [29] is used.

TABLE IV. β^- transitions in ^{80}Zn for three values of the $T = 0$ pairing strength. The contribution (in percent) of a particular configuration to the QRPA amplitude is included in parenthesis.

$V_0 = 0$ MeV ($T_{1/2} = 18.9$ s)		$V_0 = 255$ MeV ($T_{1/2} = 13.1$ s)		$V_0 = 330$ MeV ($T_{1/2} = 0.6$ s)	
$E_f - E_i$ (MeV)		$E_f - E_i$ (MeV)		$E_f - E_i$ (MeV)	
-3.088	$g_{9/2} \rightarrow g_{9/2}$ (12%) $p_{1/2} \rightarrow p_{3/2}$ (80%)	-3.271	$f_{5/2} \rightarrow f_{5/2}$ (11%) $g_{9/2} \rightarrow g_{9/2}$ (18%) $p_{1/2} \rightarrow p_{3/2}$ (60%)	-5.273	$f_{7/2} \rightarrow f_{7/2}$ (5%) $f_{5/2} \rightarrow f_{7/2}$ (71%)
-2.690	$p_{3/2} \rightarrow p_{3/2}$ (6%) $p_{1/2} \rightarrow p_{3/2}$ (11%) $f_{5/2} \rightarrow f_{5/2}$ (22%) $g_{9/2} \rightarrow g_{9/2}$ (54%)	-2.982	$f_{5/2} \rightarrow f_{5/2}$ (13%) $g_{9/2} \rightarrow g_{9/2}$ (16%) $p_{1/2} \rightarrow p_{3/2}$ (19%) $p_{3/2} \rightarrow f_{5/2}$ (47%)		
		-2.302	$p_{1/2} \rightarrow p_{1/2}$ (13%) $g_{9/2} \rightarrow g_{9/2}$ (15%) $f_{5/2} \rightarrow f_{7/2}$ (58%)		

no longer well separated and (ii) an additional transition appears, built dominantly on the back spin-flip configuration $\nu 1f_{5/2} \rightarrow \pi 1f_{7/2}$, which results in a sudden reduction of the calculated half-life. Of course, this would not be possible if $\pi 1f_{7/2}$ was fully occupied. This was the case for the Ni isotopes, and consequently their half-lives could not be improved by increasing the strength of the $T = 0$ pairing. Because the $T = 0$ pairing has a strong effect on the $\nu 1f_{5/2} \rightarrow \pi 1f_{7/2}$ configuration, a further increase of its strength lowers the energy of the corresponding transition. For $V_0 =$ 330 MeV we find only one transition, predominantly based on the $\nu 1f_{5/2} \rightarrow \pi 1f_{7/2}$ configuration.

Although $V_0 = 330$ MeV reproduces the experimental half-lives of Zn isotopes, as shown in Fig. 8, this does not mean that one should use this particular value for the other isotopic chains, even in the same mass region. This is illustrated in Fig. 9, where we display the half-lives of the $N = 50$ isotones for three values of the V_0 parameter: $V_0 = 0$ MeV, $V_0 =$ 115 MeV (used in the calculation of Fe isotopes), and $V_0 =$ 330 MeV (used for Zn isotopes). In contrast to the result of Ref. [4], the value $V_0 = 330$ MeV that reproduces the half-lives of Zn nuclei overestimates the half-life of ^{82}Ge. To reproduce the experimental value $T_{1/2} = 4.55 \pm 0.05$ s [30], the pairing strength must be increased to $V_0 = 345$ MeV. Both values, $V_0 = 330$ MeV and $V_0 = 345$ MeV, are rather close to the point at which the PN-RQRPA calculation collapses. This is illustrated in Fig. 10, where we plot the half-lives of ^{78}Zn, ^{80}Zn, ^{82}Zn, and ^{82}Ge as functions of the $T = 0$ pairing strength parameter. The PN-RQRPA instability point is, for all four nuclei, located at $V_0 \approx 400$ MeV.

B. $N \approx 82$ region

In the mass region around the doubly magic ^{132}Sn, we have calculated the β-decay half-lives of the cadmium, tin, and tellurium isotopic chains, as well as the $N = 82$ isotones. In Fig. 11 we plot the calculated half-lives of the Cd isotopes. The results correspond to two calculations, with $V_0 = 0$ and $V_0 =$ 225 MeV for the strength parameter of the $T = 0$ pairing. As in the cases that we have considered in the previous section, the

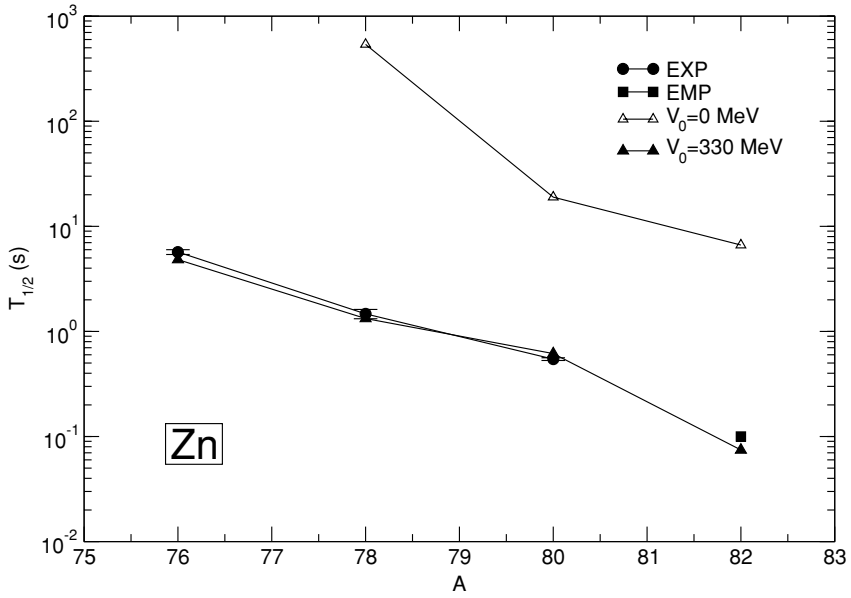

FIG. 8. Calculated half-lives of Zn isotopes, without and with the inclusion of $T = 0$ pairing in comparison with experimental and extrapolated values [30].

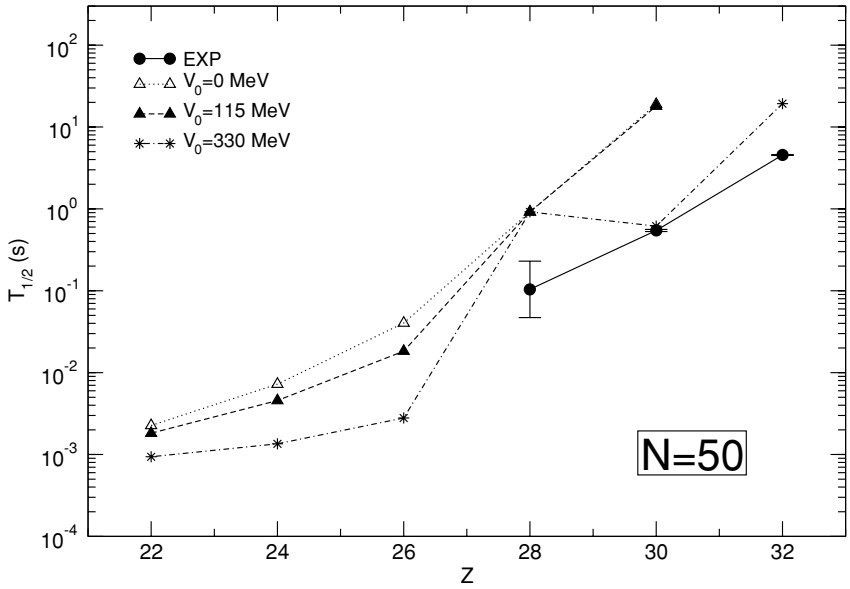

FIG. 9. Calculated half-lives of $N = 50$ isotones for three values of the $T = 0$ pairing strength. The data are from Ref. [30], except for ^{78}Ni, where the value $T_{1/2} = 104 + 126 - 57$ ms [29] is used.

calculated half-lives are more than an order of magnitude too long when the $T = 0$ pairing is not included. With the pairing strength parameter $V_0 = 225$ MeV adjusted to reproduce the half-life of ^{130}Cd, the PN-QRPA calculation reproduces the experimental half-lives of the Cd isotopic chain. With two holes in the $\pi 1g_{9/2}$ orbit, the situation in the cadmium chain is similar to that of Fe isotopes (two holes in the $\pi 1f_{7/2}$ orbit). The β-decay process in the Cd isotopes is dominated by the back spin-flip transition $\nu 1g_{7/2} \rightarrow \pi 1g_{9/2}$. Again, an increase of the $T = 0$ pairing strength partially compensates for the fact that the difference between the $\nu 1g_{7/2}$ and $\pi 1g_{9/2}$ single-particle energies is too small, due to a relatively small effective mass.

For the Sn isotopes the $\pi 1g_{9/2}$ orbit is completely occupied and the transition $\nu 1g_{7/2} \rightarrow \pi 1g_{9/2}$ is blocked. A similar problem we already encountered for the Ni isotopes. One would, therefore, expect that the calculated half-lives of the Sn isotopes will overestimate the experimental values by at least an order of magnitude, and furthermore that it will not be possible to improve the results by simply increasing the $T = 0$ pairing strength. However, this turns out to be true only for ^{132}Sn. Our model predicts that this isotope is stable against β-decay, whereas the experimental half-life is $T_{1/2} = 39.7 \pm 0.5$ s [30]. In the left panel of Fig. 12 we display the calculated half-lives of the Sn isotopes, in comparison with the available experimental data [30]. We notice that, in contrast to ^{132}Sn, the theoretical half-lives of the heavier Sn isotopes show a pronounced dependence on the $T = 0$ pairing strength. For $V_0 = 225$ MeV the calculated half-lives are only slightly longer than the experimental values. This is easily explained by the fact that in tin isotopes beyond ^{132}Sn neutrons begin to occupy the $\nu 1h_{9/2}$ single-particle level, and this enables the back spin-flip transition $\nu 1h_{9/2} \rightarrow \pi 1h_{11/2}$. The occupation probabilities of the $\nu 1h_{9/2}$ single-particle level for the Sn

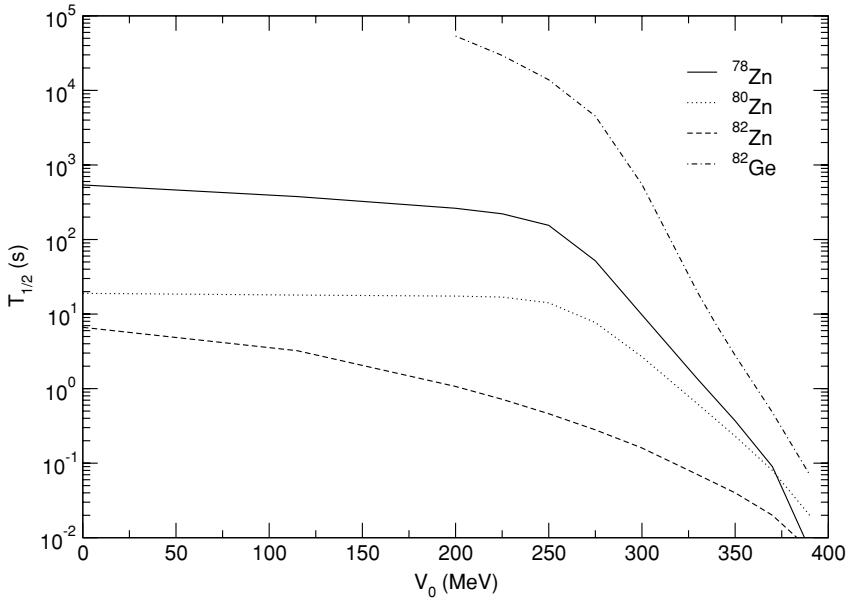

FIG. 10. Calculated half-lives of ^{78}Zn, ^{80}Zn, ^{82}Zn, and ^{82}Ge as functions of the $T = 0$ pairing strength.

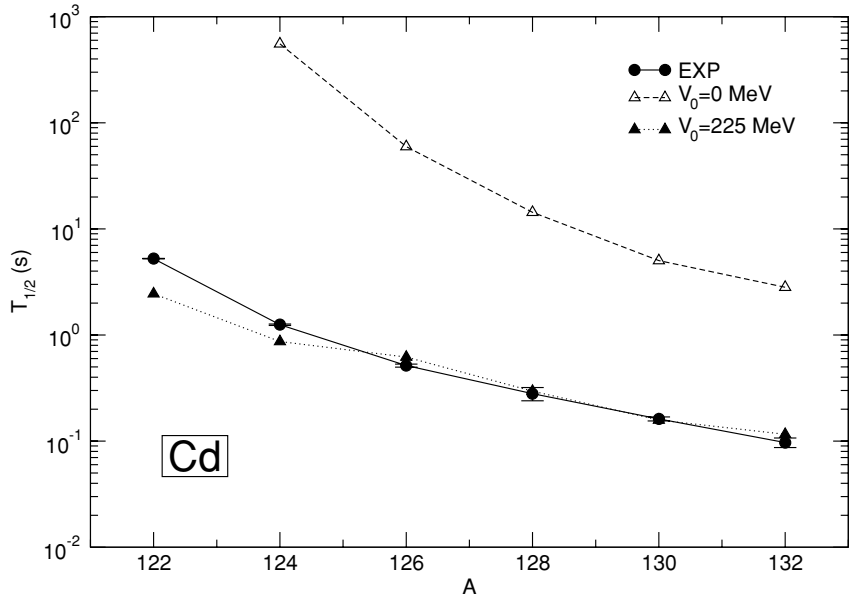

FIG. 11. Calculated half-lives of Cd isotopes for two values values of the $T = 0$ pairing strength, in comparison with available experimental data [30].

and Te isotopes are included in Table V. Because the neutron level $\nu 1h_{9/2}$ has low occupancy, the $T = 0$ pairing produces a very strong effect on the $\pi 1h_{11/2}(\nu 1h_{9/2})^{-1}$ configuration and reduces the calculated half-lives to the experimental values.

This effect is further illustrated in the middle panel of Fig. 12, where we plot the calculated half-lives of the Te isotopes in comparison with avaliable experimental data. In this case, the choice $V_0 = 225$ MeV results in half-lives that are even somewhat shorter than the experimental values. This is related to the fact that the calculated energy spacing between the $\nu 1h_{9/2}$ and $\pi 1h_{11/2}$ states in ^{132}Sn is larger than the experimental value (see Table II). A slightly lower value of the $T = 0$ pairing strength ($V_0 = 200$ MeV) accurately reproduces the half-lives of the Te isotopes. Finally, in the right panel of Fig. 12 we display the calculated half-lives of the $N = 82$ isotones compared to the shell-model results of Ref. [31]. This comparison also shows that $V_0 = 225$ MeV presents a realistic choice for the strength of the $T = 0$ pairing in this mass region.

IV. CONCLUDING REMARKS AND OUTLOOK

In this work the newly developed relativistic PN-QRPA has been for the first time applied to Gamow-Teller β decays of nuclei relevant for the r process. The matrix equations of the QRPA are formulated in the canonical single-nucleon basis of the relativistic Hartree-Bogoliubov (RHB) model. The RHB+QRPA model employed in this work is fully self-consistent. For the interaction in the particle-hole channel effective Lagrangians with density-dependent meson-nucleon couplings are used, and pairing correlations are described by the pairing part of the finite range Gogny interaction. Both in the *ph* and *pp* channels, the same interactions are used in the RHB equations that determine the canonical quasiparticle basis and in the matrix equations of the RQRPA. The model also includes a proton-neutron particle-particle interaction ($T = 0$ pairing), and here we have employed a sum of two Gaussian functions that was used in the nonrelativistic QRPA calculation [4] of β-decay rates for spherical neutron-rich r-process waiting-point nuclei.

TABLE V. Occupation probabilities of the $\nu 1h_{9/2}$ single-particle state for the ground states of the Sn and Te isotopes.

Sn		Te	
A	$v^2_{\nu 1h_{9/2}}$	A	$v^2_{\nu 1h_{9/2}}$
134	0.024	136	0.035
136	0.054	138	0.077
138	0.092	140	0.129
142	0.142	142	0.192
144	0.203	144	0.263
146	0.271	146	0.339

Microscopic global predictions of weak interaction rates are very important, because most of the neutron-rich nuclei relevant for the r-process nucleosynthesis are not accessible in experiment. Calculated β-decay half-lives depend on a detailed description of transition energies, shell structure, and on the choice of the residual interactions in the *ph* and *pp* channels. In the present analysis we have shown that standard relativistic mean-field effective interactions, adjusted to nuclear matter and ground-state properties of spherical nuclei, generally overestimate the empirical half-lives by more than an order of magnitude. The main reason is their low effective nucleon mass which, in the standard choice of interaction terms, is strongly related to the empirical energy spacings of spin-orbit partner states. Thus, to be able to reproduce measured β-decay half-lives, we have to increase the effective nucleon mass of the relativistic mean-interaction used in the RHB calculation of nuclear ground state and in the *ph* channel of the QRPA residual interaction. In this work we have done it on the mean-field level by including an additional isoscalar tensor-coupling term in the Lagrangian, which allows for an increase of the Dirac mass and effective mass while at the same time the new effective interaction reproduces the ground-state properties of finite nuclei, including the spin-orbit splittings. The new force

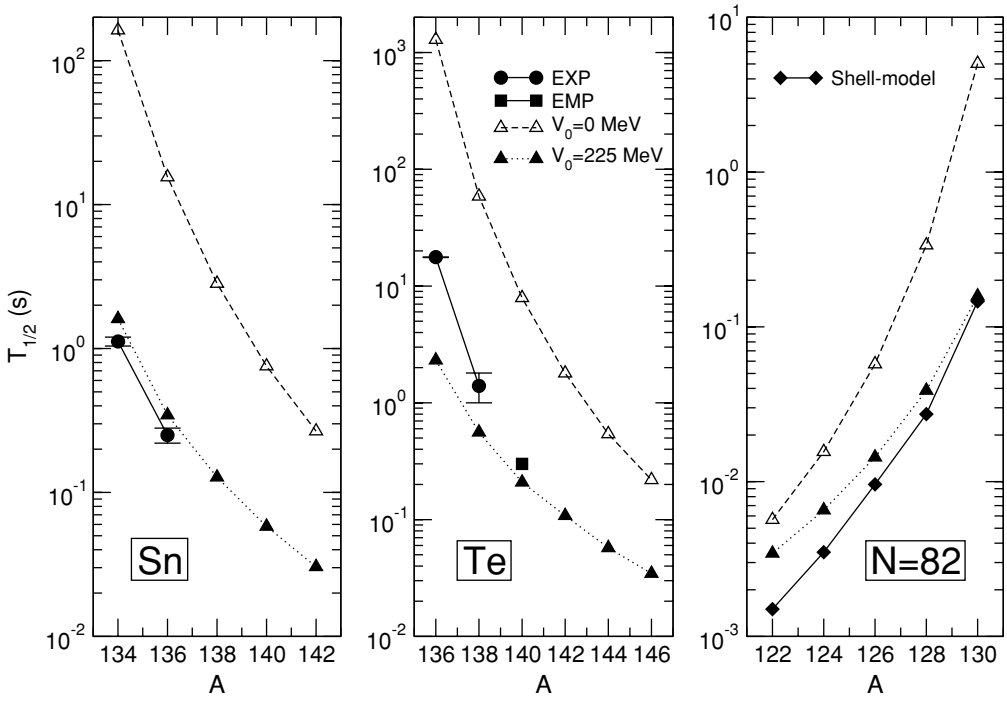

FIG. 12. Calculated half-lives of Sn (left panel) and Te (middle panel) isotopes for two values of the $T = 0$ pairing strength, in comparison with experimental data [30]. In the right panel the results for the $N = 82$ isotones are compared with the shell-model results [31].

has been adjusted starting from our most successful parameter set so far, the density-dependent interaction DD-ME1. We note, however, that the inclusion of the tensor term allows only for a moderate increase of the effective mass. We cannot, like in Skyrme forces, for example, adjust interactions with values of the effective mass close to one.

With the new density-dependent interaction DD-ME1* we have calculated the GT distribution strengths and β-decay rates of neutron-rich nuclei in the mass regions $N \approx 50$ and $N \approx 82$. The model reproduces in detail the data on GT resonances and the low-energy GT strength (see also Ref. [11]). The results for β-decay half-lives are similar to those obtained in the nonrelativistic PN-QRPA calculation of Ref. [4], where it was shown that a fine tuning of the strength of the $T = 0$ pairing interaction is necessary to reproduce the experimental data. In general, by adjusting the strength parameter of the proton-neutron pairing interaction to one experimental half-life, the PN-RQRPA calculation reproduces the data for a chain of isotopes. In the region $N \approx 50$ very different values of the $T = 0$ pairing strength reproduce the empirical lifetimes of the Fe and Zn isotopic chains, whereas a single value, adjusted to the half-life of ^{130}Cd, qualitatively reproduces the data in the $N \approx 82$ region. $T = 0$ pairing, however, does not help in the case of Ni isotopes and for ^{132}Sn, and the model overestimates the half-lives on Ni nuclei and predicts a β-stable ^{132}Sn. Therefore, we have not been able, as suggested in Ref. [4], to adjust the strength of the $T = 0$ pairing on experimental data and extend the calculation to other mass regions or even to other isotopic chains in the same mass region. This problem could be due, however, to the deficient description of shell structure, related to the low effective mass of our *ph* interaction. This is also the reason why we did not attempt a calculation of β-decay rates in the region $N \approx 126$, where there are not enough data to constrain the strength of the $T = 0$ pairing interaction.

The relativistic PN-QRPA nevertheless presents a valuable tool for the investigation of weak interaction rates of neutron-rich nuclei. It can be used for microscopic calculations not only of Gamow-Teller, but also of first-forbidden decays, which play an important role for β-decay rates both in the $N \approx 82$ and $N \approx 126$ regions [5,33]. To be able to make reliable predictions, however, the model will have to be improved by allowing for higher effective nucleon masses, possibly by going beyond the simple mean-field approximation.

ACKNOWLEDGMENTS

This work has been supported in part by the Bundesministerium für Bildung und Forschung under project 06 TM 193 and by the Gesellschaft für Schwerionenforschung (GSI) Darmstadt. N.P. acknowledges support from the Deutsche Forschungsgemeinschaft (DFG) under contract SFB 634.

[1] K. Langanke and G. Martínez-Pinedo, Rev. Mod. Phys. **75**, 819 (2003).

[2] E. Caurier, P. Navrátil, W. E. Ormand, and J. P. Vary, Phys. Rev. C **66**, 024314 (2002).

[3] N. Michel, J. Okolowicz, F. Nowacki, and M. Ploszajczak, Nucl. Phys. **A703**, 202 (2002).
[4] J. Engel, M. Bender, J. Dobaczewski, W. Nazarewicz, and R. Surman, Phys. Rev. C **60**, 014302 (1999).
[5] I. N. Borzov, Phys. Rev. C **67**, 025802 (2003).
[6] T. Nikšić, D. Vretenar, P. Finelli, and P. Ring, Phys. Rev. C **66**, 024306 (2002).
[7] T. Nikšić, D. Vretenar, G. A. Lalazissis, and P. Ring, Phys. Rev. C **69**, 047301 (2004).
[8] T. Nikšić, D. Vretenar, and P. Ring, Phys. Rev. C **66**, 064302 (2002).
[9] N. Paar, P. Ring, T. Nikšić, and D. Vretenar, Phys. Rev. C **67**, 034312 (2003).
[10] D. Vretenar, N. Paar, T. Nikšić, and P. Ring, Phys. Rev. Lett. **91**, 262502 (2003).
[11] N. Paar, T. Nikšić, D. Vretenar, and P. Ring Phys. Rev. C **69**, 054303 (2004).
[12] D. Vretenar, A. Wandelt and P. Ring, Phys. Lett. **B487**, 334 (2000).
[13] P. Ring, Zhong-yu Ma, Nguyen Van Giai, D. Vretenar, A. Wandelt, and Li-gang Cao, Nucl. Phys. **A694** (2001) 249.
[14] Z-Y. Ma, B-Q. Chen, N. Van Giai, and T. Suzuki, Eur. Phys. J. **A20**, 429 (2004).
[15] K. Ikeda, S. Fujii, and J. I. Fujita, Phys. Lett. **3**, 271 (1963).
[16] P. Ring and P. Schuck, *The Nuclear Many-Body Problem* (Springer-Verlag, New York, 1980).
[17] J. F. Berger, M. Girod, and D. Gogny, Nucl. Phys. **A428**, 25c (1984).
[18] I. N. Borzov and S. Goriely, Phys. Rev. C **62**, 035501 (2000).
[19] A. Bohr and B. R. Mottelson, *Nuclear Structure* (Benjamin, New York, 1975), Vol. II.
[20] E. J. Konopinski and M. E. Rose, in *α-, β-, and γ-Ray Spectroscopy*, edited by K. Siegbahn (North-Holland, Amsterdam, 1965), p. 1327.
[21] C. Mahaux and R. Sartor, Adv. Nucl. Phys. **20**, 1 (1991).
[22] P.-G. Reinhard, Nucl. Phys. **A649**, 305c (1999).
[23] M. Jaminon and C. Mahaux, Phys. Rev. C **40**, 354 (1989).
[24] M. Jaminon and C. Mahaux, Phys. Rev. C **41**, 697 (1990).
[25] D. Vretenar, T. Nikšić, and P. Ring, Phys. Rev. C **65**, 024321 (2002).
[26] R. J. Furnstahl, J. J. Rusnak, and B. D. Serot, Nucl. Phys. **A632**, 607 (1998).
[27] V. I. Isakov, K. I. Erokhina, H. Mach, M. Sanchez-Vega, and B. Fogelberg, Eur. Phy. J. **A14**, 29 (2002).
[28] S. Franchoo *et al*., Phys. Rev. Lett. **81**, 3100 (1998).
[29] P. Hosmer, contribution to the International Nuclear Physics Conference, INPC2004, Göteborg, Sweden.
[30] NUBASE database, for availability via Internet see Atomic Mass Data Center, http://csnwww.in2p3.fr/amdc.
[31] G. Martinez-Pinedo and K. Langanke, Phys. Rev. Lett. **83**, 4502 (1999).
[32] NUDAT database, National Nuclear Data Center, http://www.nndc.bnl.gov/nndc/nudat/
[33] J. Shergur *et al*., Phys. Rev. C **65**, 034313 (2002).